# The effect of spatial resolution on the in-cloud atmospheric icing conditions in numerical weather model at the Fargernes mountain, Norway

Yngve Birkelund[1], Pravin Punde[1], Jonas Mundheim Strand[1,2]

[1] *UiT The Arctic University of Norway, Norway*
[2] *Kjeller Vindteknikk, Norway*

yngve.birkelund@uit.no, pravin.b.punde@uit.no, jonas.m.strand@uit.no

*Abstract*— **Atmospheric icing poses significant risks to infrastructure, aviation, and the energy section. Numerical weather models, as the Weather Research and Forecasting model (WRF), can be used to describe the atmospheric conditions relevant for atmospheric icing. In this study, we will focus on the Fagernes mountain meteorological icing measurement site where the WRF model is set up using ERA5 input data, Thompsons microphysics scheme to describe the different hydrometeors, and the Yonsei University (YSU) planetary boundary scheme with increasing spatial resolutions from 9, 3 and 1 km resolution. The final high-resolution model is using a Large Eddy Simulation (LES) for planetary boundary layer option in WRF with 91 m horizontal resolution in the model, in which a 10 m digital elevation model of Norway is used as model input.**

**Using supercooled liquid water content, we have shown that the increased resolution from 9 to 1 km clearly changes the atmospheric conditions in the numerical model at the Fagernes mountain icing rig site. The main reason for this change seems to be that higher resolution models provides a better representation of the true terrain. Since the icing rig is located on a mountain top, the model height of the site does increase as the model spatial resolution increases.**

**Introducing the high-resolution LES model, both the mountain height the surrounding terrain is clearly closer to the real terrain at the measurement site. The LES model provides very good results for studying single or short time icing events and allows for a better understanding of the local terrain effects when in comes to atmospheric icing. The increased computational cost of the LES model makes it difficult use for larger areas and/or for long time simulations.**

Keywords— ***WRF, numerical weather models, large eddies simulations, icing measurements.***

## I. Introduction

Numerical weather prediction models (NWP) describe the physical weather parameters in the atmosphere, at the surface and in the soil. The physical relationship for the parameters is given as mathematical equations that are solved numerically, or in cases where meteorological processes are small scale or complex, solved using different parameterizations. For atmospheric icing, some of the important weather parameters are temperature, liquid water content and wind speeds.

With an established mathematical model of the atmosphere, the NWP model need to be initialized with information about the terrain at the place under study as well as the current state of atmosphere. Measurement from both ground stations, satellites and radiosondes are collected, and in most cases shared between meteorological organizations, to create a global coverage of standardized measurements of the current weather. After initialization, the NWP model can be used to estimate the historical, current or future state of the atmosphere, or at any place around the globe. The numerical model is based on Examples of operational weather forecast services are the Integrated Forecasting System (IFS) from the European Centre for Medium-Range Weather Forecast (ECMWF) and the Global Forecast System (GFS) from the NOAA Environmental Modeling Center in US, both models are updated four times a day with a horizontal resolution/ forecast length of 15days/9km and 16days/13km, respectively.

The Weather and Research Forecasting model (WRF) is an open community model by the National Center for Atmospheric Research [1]. This model can be configured with several different physical schemes options, and both research and industry users have been using this for a wide range of applications as e.g. wind resource assessment [2,3], wildfire tracking [4] and icing [5,6].

## II. Method

### A. Fagernes mountain icing measurement station

The icing measurement station is at the Fagernes mountain in Northern Norway as shown in Fig. 1. The location is at 1013 m asl, at latitude 68.4206N and longitude 17.4851E, with steep dropoff to sea-level at the fjords Beisfjorden to the south and Rombaken to the north. The city of Narvik is located nearby to the west, and several mountain peaks nearby to the east. Note that a power line (black line) passes close to this location, and also telecommunication masts and ski lift are in within a 100 meters distance. Earlier winters has shown that all this infrastructure is prone to icing, and we will look on a measured icing event during November 29.-30. 2022.

The location is above the Arctic circle, and in a coastal region with open ocean to west, a complex terrain with several fjords and mountains for several kilometres in all directions, and flat and in-land climate further to the east. Low pressure systems typically bring precipitation from the ocean during winter season, while easterly wind is cold and dry.

Measurements every10 min are used for this station, and in this paper we will focus on temperature, relative humidity, pressure, wind speed and icing rates on a standard cylinder.


Fig. 1 Location of measurement mast (orange marker) and nearby terrain features. Map from: www.norgeskart.no

### B. *WRF setup*

WRF version 4.4 was configured with physics schemes as shown in Table 1. The model was initialized with hourly ERA5 data from ECMWF, and run from 28.10.2022 12:00 to 31.10.2022 00:00 to cover an icing event captured at the icing measurement station.

The nesting ability of WRF was used for domains of size 103x103 cells with increasing horizontal resolution of 9, 3, 1 km for domain 01-03, respectively, shown in Fig. 2, with terrain data from Global Multi-resolution Terrain Elevation (GMTED) at 30 arcsec. Due to the complex terrain in the region, the number of vertical levels was set to 121 and the timesteps for the numerical simulation was set to 3*DX to avoid CFL-errors. The final high-resolution simulation in domain 04 consisted of 199x199 cells with 90,9 m horizontal resolution, shown in Fig. 3. using a 10m resolution digital elevation model from the Norwegian Mapping Authority [13] and converted to WRF format.

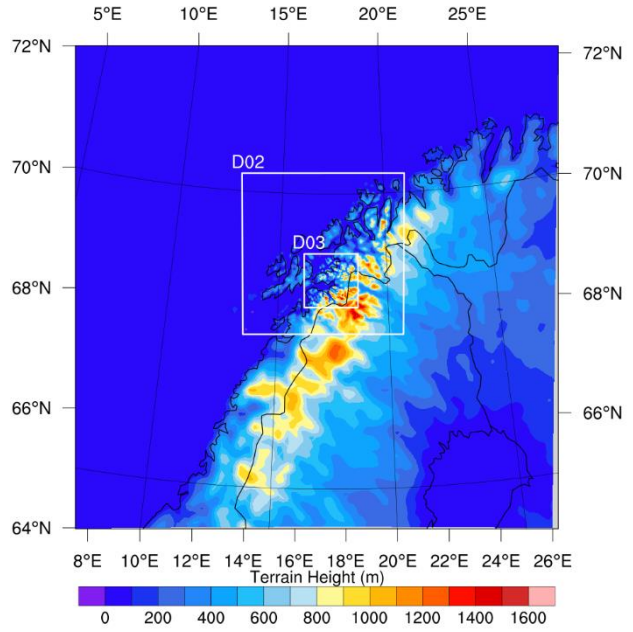


Fig. 2 WRF domains D01 (large plot), D02 and D03. Color code within each domain corresponds to its model terrain heights.

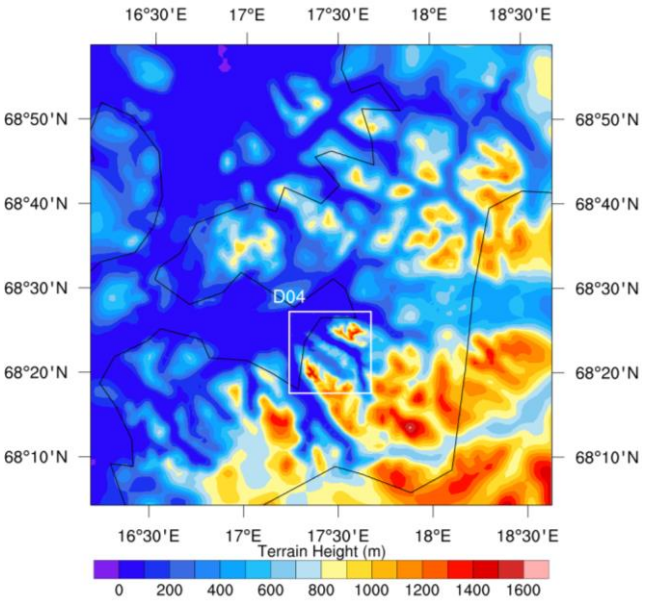


Fig. 3 Location and terrain of D03 and D04 (LES) in WRF. Black lines show global sea-land mask and the border between Norway and Sweden.

TABLE I. WRF CONFIGURATION

| Physics | Scheme (opt) | Domains | Reference |
|---|---|---|---|
| Microphysics | Thomson (8) | 01-04 | [7] |
| Long/shortwave radiation | RRTMG (4) | 01-04 | [8] |
| Cumulus | Kain-Fritsch (1) | 01-03 | [9] |
| Planetary boundary layer | YSU (1) | 01-03 | [10] |
| | LES (0) | 04 | |
| Surface physics | MM5 (1) | 01-04 | [11] |
| Land-surface | Noah (2) | 01-04 | [12] |

### C. *WRF simulations and post-processing*

Simulations were run on the Fram supercomputer through the Sigma2 national e-infrastructure in Norway. The first 3 domains was run without feedback between the domains, and the LES domain was run using this NDOWN option with D03 as input. Dynamic options includes: w_damping=1, diff_opt=2 and epssm=0.1. For the LES simulation epssm was increased to 0.8, and mix_isotropic=1 was applied.

To allow for a direct comparison of results from all domains, the WRF outputs are interpolated to the exact location of the measurement mast using wrf-python scripts.

The icing rate is calculated using Makkonens model for a cylinder [14]

$$\frac{dM}{dt} = \alpha_1 \alpha_2 \alpha_3 \omega v A \,. \quad (1)$$

Here $M$ is the ice mass, $\omega$ mass concentration of hydrometeors (typically supercooled liquid water content), $v$ the wind velocity and $A$ the cross-section of the cylinder. The $\alpha$- terms are for collision, sticking and accretion efficiency, respectively. More details about measurement, calculation of these parameters and the WRF icing rate can be found in the companion papers [15,16].

## III. Results

### A. *Terrain heights and model resolution*

The true terrain is shown in Fig. 4 a) together with the WRF model terrains in Fig. 4 b)-d) all for the inner domain. This region covers an area of 18x18 km, and the terrain is highly complex with several steep cliffs, narrow fjords and sharp mountain peaks.

When using a model with 3km resolution the terrain is clearly smoothed so that both lower terrain features as fjords as well as mountain peaks have disappeared within this region. A model resolution of 1km, as in the case of D03 in Fig. 4 c), gives a better resemblance to the valleys/fjords but still the height of the measurement station is more than 200 meter too low compared to its true height. The height difference is connected to the narrow mountain ridge the station is located on.

The high-resolution LES model shown in Fig. 4 d), on the other hand, clearly shows all peaks and fjords, and the height difference at the measurement rig is less than 10 meters.

### B. *Icing event time series*

Fig. 5 shows the time series of measurements and WRF results at the measurement station during the period Nov 29th at 00:00 to Nov. 31st, 2022. Note that color code for the model output are the same in all plots in this figure, although the legend is only shown in second and fourth plot to avoid masking the data.

The measured temperature (T) shown in upper row of Fig. 5 starts at 0°C, drops down to -5°C during the first day before it rises again. The model outputs all follow the same time dependency, but with different levels for each domain. The D01 has temperature approx. +4°C compared to the measurements, while D02-D04 are approx. +2, 0, -1°C, respectively. These temperature level differences have a direct and strong connection to the model terrain heights, which increases as the resolution increases.

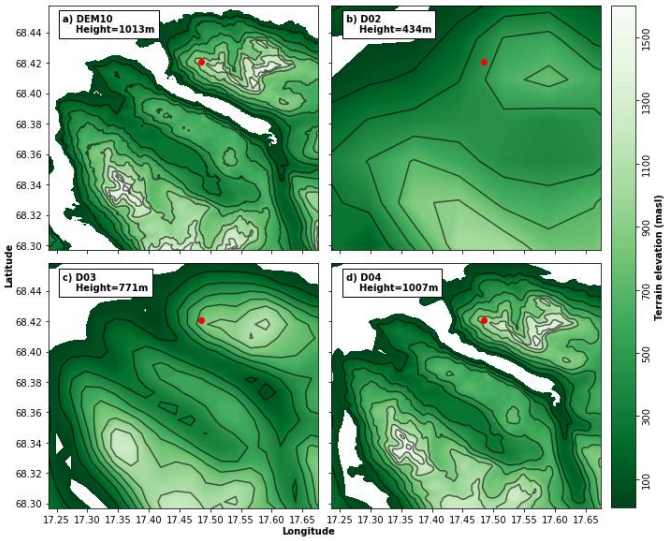


Fig. 4 Terrain heights using a) Digital elevation model of Norway - 10 m resolution, b) WRF D02 - 3 km, c) WRF D03 – 1 km, d) WRF D04 – 90,9m. Green colorscale shows height above sea level, contour lines are shown every 200 m from 100 masl to 1500 masl. Red markers give location of the measurement mast, and its corresponding model height is shown in the text box

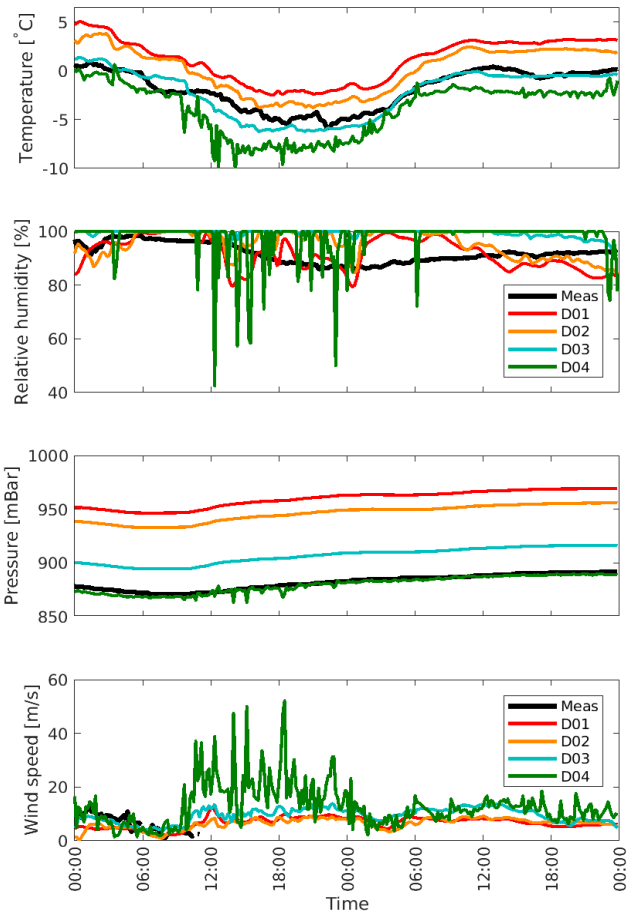


Fig. 5 Measurement (black lines) and model result from D01 (red), D02 (orange), D03 (blue), D04 (green). Temperature, relative humidity, pressure, and wind speed in row 1-4, respectively

Relative humidity (RH) during this event, shown in second row of Fig. 5, have measurement in the range from 85% to 99%, with its lowest values in the middle of the event from 29.10 18:00 – 30.10 06:00. The model results are mostly in the same range, but some deviations are clearly visible. First, the modelled RH varies up-and-down several time during this event, most notably for the D04 case where the drop in RH can be down to 40% for single time steps. Second, during the last day the model tends to decrease RH while the measurements show a slowly increasing trend.

The pressure results, shown in third row of Fig. 5, shows a very good fit between the measurements and the D04 model result. This is expected as the model height is almost the same as the true terrain height for this domain, while the D01-D03 results shows higher pressure directly related to their respective model height at this spot.

The last row of Fig. 5 shows the wind speed results. The measurement in this event stops around 11:00 this first day, a disturbing but not uncommon problem during icing events. The anemometer is heated, but the misfunction was probably a result of strong cooling from the combination of temperature and wind. While working, the measurements are close to the D03 and D04 results, while both D01 and D02 shows lower wind speeds. Results from D04 have clearly higher wind speeds compared to the other domains, but, as in the case of RH model results, the variation is very large as the wind speed jumps between 20-50 m/s. The road authorities have measurements at Gratangsfjellet (334 masl, 68.67N, 17.90E) which shows wind gust of 33 m/s at these times.

The ice load measurement is shown in Fig. 6 as a red line. Measurements are saved every minute, and the data has high variation with a build up of ice on the cylinder starting from approximately 10:00 the first day. This matches well with the sharp increase in wind speed shown in Fig. 5. To reduce noise, the ice load time series was filtered with a low pass Chebyshev filter of 8th order with cut-off frequency $f_c = 0.8\,\frac{fs}{2}\frac{1}{60}$, and the resulting hourly icing load is shown as the light green line in Fig. 6. From this a first order difference is used to create an estimate of the icing rate, shown as black line in Fig. 6.

Going from ice load measurement to icing rate is a difficult task, as it is difficult to distinguish between e.g. measurement noise, ice accretion and ice shredding on the cylinder. As the temperature during this event is below zero, no melting are expected but the ice/snow build up on the cylinder is most likely falling of piecewise during the ice accretion phase.

Fig. 7. show the icing rate results using the WRF model for domain D01-D04. In the lowest resolution domains, D01 and D02, produce almost no icing, while both D03 and D04 give icing rates that confirms the icing event. Note that both these domain give quite high icing from 03:00-15:00 the second day, while the ice load measurement only shows small loads (red line, 1 min measurements in Fig 6). In addition, the average level of icing rates during the first day indicates that the D03 results are below the measurement results, while the D04 results are above and at two points all the way up to 1600 g/h.

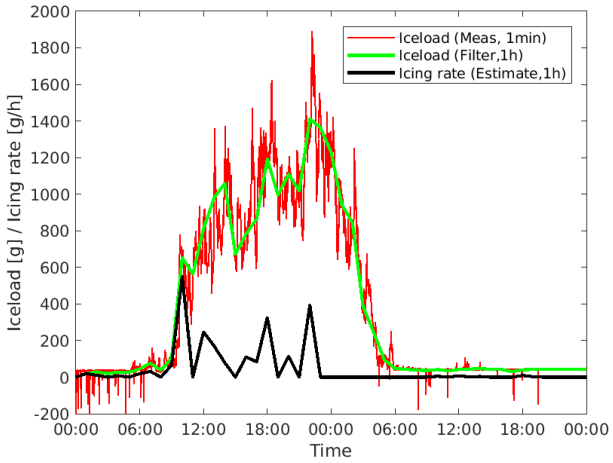


Fig. 6 Ice load measurements and estimated icing rate.

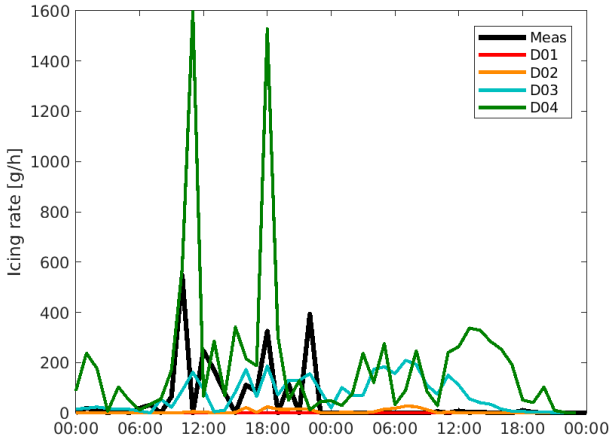


Fig. 7. Icing rate results from ice load measurement and WRF modelling using domain D01-D04.

### *C. Liquid water content during icing event*

The upper row of Fig. 8 shows the horizontal wind speed, wind direction and liquid water content (LWC) contour lines from WRF domain D03 and D04, to the left and right, respectively. Results are from the lowest model layer, at approximately 20magl, from 29.10.2022 at 11:00 in the beginning of the measured icing event.

Starting with the wind results from D03, the main wind direction is from the north. The mountains north of the measurement station provides some shadowing effects so that lower-level terrain as e.g. the fjord experience lower wind speeds. Further inland, the wind tends to turn to the east. This is particularly the case along fjords going in this direction. Wind speeds and directions in D04 is much more complex, as LES captures smaller structures so that wind follows the terrain, changes directions several places, and we typically find much higher wind speeds over mountains. Results from other nearby output times, not shown, further elaborate the difference between D03 and LES (D04), as time steps in D03 typically have similar results while LES results may change significantly for our time step during rough weather events.

The LWC in these results clearly indicates that mountain areas, where temperature drops, are prone to icing at this time. In D03 we find LWC above 1 g/kg at some spots, while the D04 icing rates could be twice as high. Looking near the measurement station, shown as yellow circle in these plots, we find that the whole mountain is within a 1g/kg level, and also a nearby 1.5g/kg contour line.

The low row of Fig. 8 shows a vertical cross section along the south-north line crossing the measurement station. The terrain height is shown with brown region below, and the dotted temperature lines in D03 gives a freezing temperature level at 0°C around 500 masl. Below this line no icing would normally occur. The mountains do create some movement of air vertically, as also can be seen on the temperature isobars. When going LES and D04, the high wind speed can be seen over a large vertical distance, and we also find strong variations spatially both for temperature, wind and LWC. At this instant, our results indicate heavy icing potential from the measurement station and all the way up to 3000 masl.

## IV. Conclusions

We have shown that the horizontal resolution in the weather model has a strong impact on the estimated icing rate, and we have identified two important reasons for this: 1) A higher resolution in the model is better able to reproduce the true terrain features, and 2) LES modelling allows for capturing high wind events which may produce short time icing conditions with extreme high icing rates.

Some concerns and limitations: a) High resolutions and extreme weather conditions means that we need high computation power as well as analysing output with high temporal resolution. b) The WRF output in this paper are instantaneous values and does not include averaging as in the measurement cases c) Our results are only for a single station, for a short event, and finding should thus only be read as indication of trends when moving into LES modelling for icing.

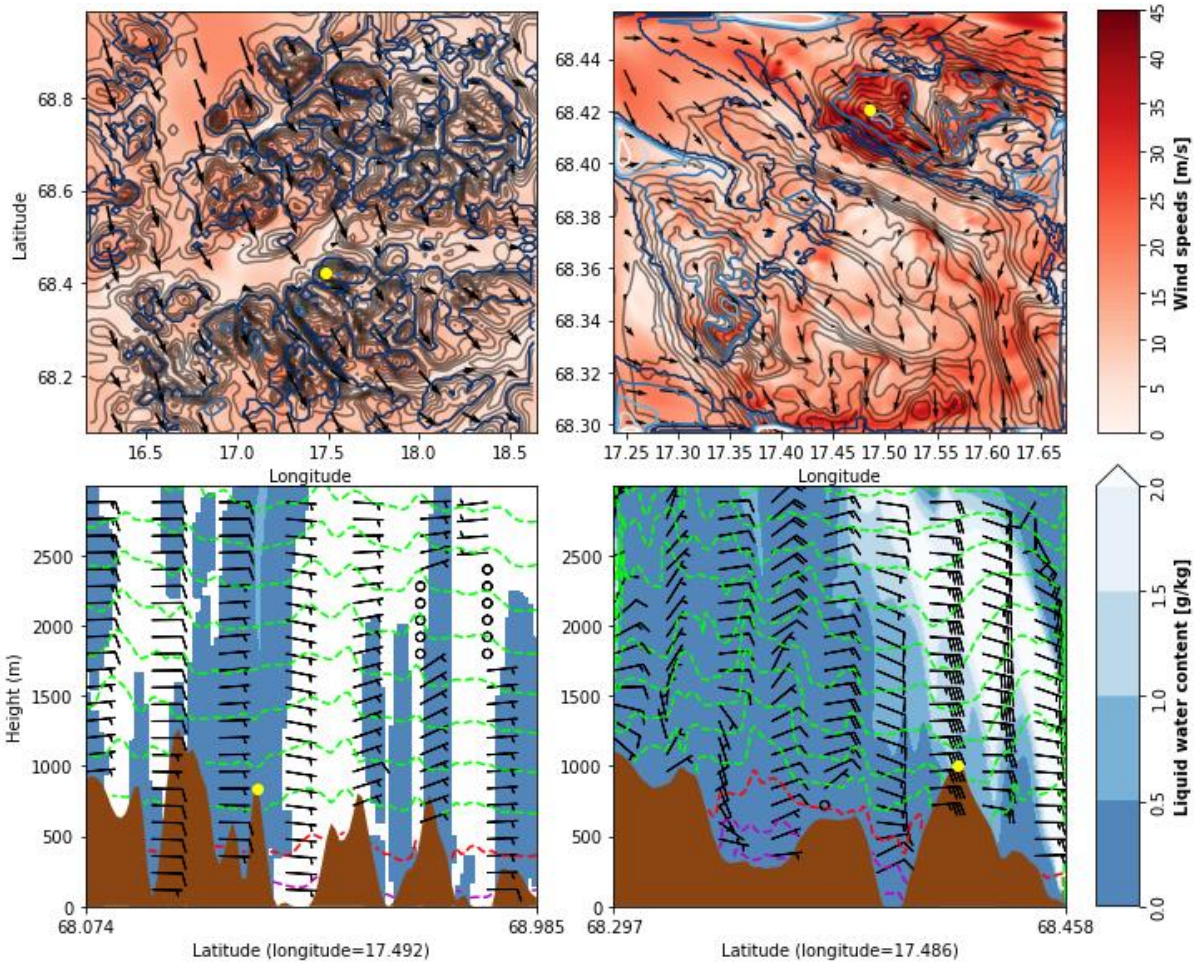


Fig. 8. Liquid water content (blue/filled contour) and wind speeds (red filled contour) from WRF. Upper row lowest horizontal model plan (~20 magl), lower row cross section plan south-north through model station (yellow circle). Left: D03, right: D04. Temperature contours: 0°C (red dotted line), +2 increase (dotted magenta line), -2 decrease (dotted cyan line). Wind direction shown with quiver and barbs.


## ACKNOWLEDGMENT

The work reported in this paper is supported by nICE project (Project no-324156) funded by UiT & Research Council of Norway. The simulations were run on resources provided by Sigma2 – The National Infrastructure of High-Performance Computing and Data Storage in Norway.


## REFERENCES


[1] Skamarock, W. C., Klemp, J. B., Dudhia, J., Gill, D. O., Liu, Z., Berner, J., Wang, W., Powers, J.G., Duda, M.G., Barker, D. and Huang, X. (2021). "A Description of the Advanced Research WRF Model Version 4.3" (No. NCAR/TN-556+STR)

[2] Hahmann, A.N., Sïle, T., Witha, B., Davis, N.N., Dörenkämper, M., Ezber, Y., García-Bustamante, E., González-Rouco, F., Navarro, J., Olsen, B.T. and Söderberg, S. (2020). "The making of the New European Wind Atlas-Part1 Model sensitivity", Geoscientific Model Development, 13(10), pp 5053-5078.

[3] Anacona, H.W., Mattar, C., Alonso-de-Linaje, N.G., Sepúlveda, H.H. and Crisóstomo, J. (2023). "Wind simulations over western Patagonia using the Weather Research and Forecasting model and reanalysis" Atmosphere 14, no. 7: 1062.

[4] A. Bakhshaii and E.A. Johnson. 2019. "A review of a new generation of wildfire–atmosphere modeling", Canadian Journal of Forest Research. 49(6): 565-574.

[5] Kringlebotn Nygaard, B. E., J. E. Kristjánsson, and L. Makkonen, 2011: Prediction of In-Cloud Icing Conditions at Ground Level Using the WRF Model. J. Appl. Meteor. Climatol., 50, pp 2445–2459

[6] Federico, S., Díaz-Fernández, J., Quitián-Hernández, L., Bolgiani, P., Santos-Muñoz, D., García Gago, Á., Fernández-González, S., Valero, F., Merino, A., García-Ortega, E., Sánchez, J.L., Sastre, M., Martín, M.L. (2020) "Mountain Waves Analysis in the Vicinity of the Madrid-Barajas Airport Using the WRF Model", Advances in Meteorology

[7] Thompson, G., P. R. Field, R. M. Rasmussen, and W. D. Hall, (2008) Explicit Forecasts of Winter Precipitation Using an Improved Bulk Microphysics Scheme. Part II: Implementation of a New Snow Parameterization. Mon. Wea. Rev., 136, 5095–5115,

[8] Iacono, M. J., J. S. Delamere, E. J. Mlawer, M. W. Shephard, S. A. Clough, and W. D. Collins (2008), Radiative forcing by long-lived greenhouse gases: Calculations with the AER radiative transfer models, J. Geophys. Res., 113, D13103

[9] Kain, J. S., 2004: The Kain–Fritsch Convective Parameterization: An Update. J. Appl. Meteor. Climatol., 43, 170–181

[10] Hong, S., Y. Noh, and J. Dudhia, 2006: A New Vertical Diffusion Package with an Explicit Treatment of Entrainment Processes. Mon. Wea. Rev., 134, 2318–2341

[11] Jiménez, P. A., J. Dudhia, J. F. González-Rouco, J. Navarro, J. P. Montávez, and E. García-Bustamante, 2012: A Revised Scheme for the WRF Surface Layer Formulation. Mon. Wea. Rev., 140, 898–918

[12] Tewari, M., Chen, F., Wang, W., Dudhia, J., LeMone, MA., Mitchell, K., Ek, M. Gayno, G., Wegiel,J. Cuenca, R.H., 2004. Implementation and verification of the unified Noah land surface model in the WRF model, 20th Conf. on Weather Analysing and Forecasting, 2165–2170

[13] (2023) The Norwegian Mapping Authority website [Online] https://hoydedata.no/

[14] Makkonen, L., 2000: "Models for the Growth of Rime, Glaze, Icicles and Wet Snow on Structures". *Philosophical Transactions: Mathematical, Physical and Engineering Sciences*, *358*(1776), 2913–2939.

[15] Punde, P., Birkelund, Y., Virk, M.S., Han, X. 2024: "In-Cloud Icing - A case study at Fagernesfjellet, Norway using Weather Research and Forecasting model and observations", IWAIS 2024

[16] Strand, J.S., Birkelund, Y., Punde, P., 2024: "Atmospheric In-cloud Icing Using WRF for an Alpine Wind Power Plant in Norway", IWAIS 2024